

# Linear dependence of $T_c$ on inter-site attraction in two-dimensional extended Hubbard model

Zhipeng Sun\*

*Beijing Computational Science Research Center, Beijing 100193, China*

Hai-Qing Lin<sup>†</sup>

*Beijing Computational Science Research Center, Beijing 100193, China and  
School of Physics, Zhejiang University*

(Dated: April 18, 2023)

Recent experimental studies suggest that the minimal model for describing cuprate superconductors is an extended Hubbard model with strong on-site repulsion and nearest-neighbor attraction. This article studies the behavior of the superconducting critical temperature  $T_c$  for this model using mean-field theory, assuming that above  $T_c$  the system is in a pure antiferromagnetic or Fermi liquid phase, and below  $T_c$  the superconducting order is subject to the spatial modulation. The mean-field analysis reveals the fundamental difference between cuprates and conventional metal-based superconductors, namely that the energy scale of the effective bandwidth is comparable to  $T_c$ , resulting in an almost linear dependence of optimal  $T_c$  on the nearest-neighbor attraction. Therefore, the mean-field theory provides a good qualitative description of the superconducting problem in the extended Hubbard model and suggests that sufficiently narrow bands and strong attractions are the two key factors for designing high- $T_c$  superconducting materials.

The high- $T_c$  superconductivity (SC) mechanism in the cuprates is a long standing problem in condensed matter physics, and the origin of effective pairing attraction is at the heart of the issue [1–5]. The Hubbard model, proposed as the simplest model for explaining the high- $T_c$  SC mechanism [6], has achieved remarkable success in explaining various phenomena in the cuprates, including the antiferromagnetism (AFM) [7], the pseudogap [8, 9] and the strange metallic behavior [10, 11]. However, there is still a great controversy on whether SC exists in the Hubbard model [12–14], namely whether the Hubbard model is the minimal model for cuprate superconductors remains a question. Recent experimental results on the one-dimensional cuprate chain [15] confront with the simple Hubbard model, and suggest the extended Hubbard model with nearest-neighbor attraction, likely originating from the electron-phonon interaction [15, 16], as the minimal model describing the cuprate chain. This experimental result has led to research on the SC problem in the one- and two-dimensional extended Hubbard model [17, 18], particularly the role of local repulsion and nearest-neighbor attraction.

The role of intersite attraction in the SC problem on the extended Hubbard model was investigated early on by Micnas in 1988 within the mean-field framework [19]. Specifically, it was found to provide an effective attraction between two nonlocal pairings, thereby inducing the  $d$ -wave,  $p$ -wave, and extended  $s$ -wave pairing instabilities. However, the impact of the local repulsion on the SC problem remains unclear, as it was assumed to be small and negligible in this literature [19]. A more crucial question is, whether there is a fundamental difference between SC in the extended Hubbard model and conventional superconductors [20, 21].

Aiming at these questions, we revisit the SC problem in the extended Hubbard model with strong onsite repulsion  $U$  and nearest-neighbor attraction  $|V|$ , under the mean-field framework. In consideration of the strong local repulsion, the system is assumed in either a pure AFM phase or Fermi liquid phase above  $T_c$ . Due to the AFM arrangement of fermions, the SC order below  $T_c$  is also subject to spatial modulation. The SC gap equations near  $T_c$  are then constructed based on these assumptions, and thus  $T_c$  can be determined. The theoretical analysis of the limiting AFM case indicates that the effective bandwidth  $D$  becomes extremely narrow owing to the large AFM gap. If the energy scale of  $D$  is comparable to  $T_c$ ,  $T_c$  obtained from the SC gap equation will be nearly linear in  $|V|$ , which is totally different from its behavior in the conventional superconductors. We confirm our theoretical analysis by numerical results under various parameters.

**Model and methods.** We investigated the extended Hubbard model with strong onsite repulsion and nearest-neighbor attraction on a two-dimensional square  $\mathcal{V} = L \times L$  lattice, whose Hamiltonian reads

$$\hat{H} = -t \sum_{\alpha, \mathbf{r}, \boldsymbol{\delta}} \hat{c}_{\alpha, \mathbf{r}+\boldsymbol{\delta}}^\dagger \hat{c}_{\alpha, \mathbf{r}} - \mu \sum_{\mathbf{r}} \hat{\rho}_{\mathbf{r}} + U \sum_{\mathbf{r}} \hat{n}_{\uparrow, \mathbf{r}} \hat{n}_{\downarrow, \mathbf{r}} - \frac{|V|}{2} \sum_{\mathbf{r}, \boldsymbol{\delta}} \hat{\rho}_{\mathbf{r}+\boldsymbol{\delta}} \hat{\rho}_{\mathbf{r}}. \quad (1)$$

Here  $\hat{c}_{\alpha, \mathbf{r}}^\dagger$  ( $\hat{c}_{\alpha, \mathbf{r}}$ ) is the fermionic creation (annihilation) operator with spin  $\alpha$  at lattice site  $\mathbf{r}$ ,  $\hat{n}_{\alpha, \mathbf{r}} \equiv \hat{c}_{\alpha, \mathbf{r}}^\dagger \hat{c}_{\alpha, \mathbf{r}}$  is the spin-selective density operator, and  $\hat{\rho}_{\mathbf{r}} = \hat{n}_{\uparrow, \mathbf{r}} + \hat{n}_{\downarrow, \mathbf{r}}$  is the charge density operator.  $\boldsymbol{\delta}$  represents the vectors linking nearest neighbors,  $t$  is the nearest-neighbor hop-

ping strength,  $U$  is the onsite repulsion,  $|V|$  is the nearest-neighbor attraction, and  $\mu$  is the chemical potential.

Within the standard Hartree-Fock framework, we make ansatz for several mean fields. The mean spin density  $m_{\mathbf{r}}$ , defined as  $\frac{1}{2} \langle \hat{n}_{\uparrow\mathbf{r}} - \hat{n}_{\downarrow\mathbf{r}} \rangle$  is assumed to take the form  $m_{\mathbf{r}} = m e^{i\mathbf{Q}\cdot\mathbf{r}}$  with  $m \geq 0$  and  $\mathbf{Q} = (\pi, \pi)$ . That means, above  $T_c$ , the system is in either the AFM phase or Fermi liquid phase. The mean charge density  $\rho_{\mathbf{r}} = \langle \hat{\rho}_{\mathbf{r}} \rangle$  is assumed to be uniform in space, i.e.  $\rho_{\mathbf{r}} = \rho$ , which means the charge density wave (CDW) order is not in consideration. The intersite mean field  $n'_{\alpha,\delta,\mathbf{r}}$ , defined as  $\langle \hat{c}_{\alpha,\mathbf{r}}^\dagger \hat{c}_{\alpha,\mathbf{r}+\delta} \rangle$ , is simply assumed as

a scalar  $\frac{1}{2}\rho'$ . The local SC mean field  $\Delta_{\mathbf{r}}$ , defined as  $\langle \hat{c}_{\downarrow,\mathbf{r}} \hat{c}_{\uparrow,\mathbf{r}} \rangle$ , is assumed as a scalar  $\Delta$ . The intersite unequal-spin SC mean field  $\Delta'_{\delta,\mathbf{r}}$ , defined as  $\langle \hat{c}_{\alpha,\mathbf{r}}^\dagger \hat{c}_{\alpha,\mathbf{r}+\delta} \rangle$ , is assumed to be subject to spatial modulation due to the AFM arrangement of fermions, and thus takes the form:  $\Delta'_{\delta,\mathbf{0}} + \Delta'_{\delta,\mathbf{Q}} e^{i\mathbf{Q}\cdot\mathbf{r}}$ . The nonlocal equal-spin SC mean field  $\Delta'_{\alpha,\delta,\mathbf{r}} = \langle \hat{c}_{\alpha,\mathbf{r}+\delta} \hat{c}_{\alpha,\mathbf{r}} \rangle$ , whereas, is assumed to be zero here. By these ansatz, the mean-field Hamiltonian is then reduced to  $\hat{H}_{\text{MF}} = \sum_{i,j,\mathbf{p}} \hat{c}_{\mathbf{p}}^{i\dagger} h_{\mathbf{p}}^{ij} \hat{c}_{\mathbf{p}}^j$ , where  $\mathbf{p}$  is confined in the half of the first Brillouin zone,  $\hat{c}_{\mathbf{p}}^{i\dagger}$  represents for  $\left[ \hat{c}_{\uparrow,-\mathbf{p}}^\dagger, \hat{c}_{\uparrow,-\mathbf{p}+\mathbf{Q}}^\dagger, \hat{c}_{\downarrow,\mathbf{p}}, \hat{c}_{\downarrow,\mathbf{p}+\mathbf{Q}} \right]$ , and  $h_{\mathbf{p}}$  is a  $4 \times 4$  matrix given by

$$h_{\mathbf{p}} = \begin{bmatrix} -2\tilde{t}\gamma_{\mathbf{p}} - \tilde{\mu} & -Um & U\Delta - |V|X_{\mathbf{0},\mathbf{p}} & -|V|X_{\mathbf{Q},\mathbf{p}} \\ -Um & 2\tilde{t}\gamma_{\mathbf{p}} - \tilde{\mu} & |V|X_{\mathbf{Q},\mathbf{p}} & U\Delta + |V|X_{\mathbf{0},\mathbf{p}} \\ U\Delta^* - |V|X_{\mathbf{0},\mathbf{p}} & |V|X_{\mathbf{Q},\mathbf{p}} & 2\tilde{t}\gamma_{\mathbf{p}} + \tilde{\mu} & -Um \\ -|V|X_{\mathbf{Q},\mathbf{p}} & U\Delta^* + |V|X_{\mathbf{0},\mathbf{p}} & -Um & -2\tilde{t}\gamma_{\mathbf{p}} + \tilde{\mu} \end{bmatrix}. \quad (2)$$

Here  $\tilde{t}$  stands for the renormalized nearest-neighbor hopping strength  $t - \frac{1}{2}|V|\rho'$ ,  $\tilde{\mu}$  stands for the renormalized chemical potential, and  $\gamma_{\mathbf{p}} = \cos p_x + \cos p_y$  is an  $s$ -wave symmetric function. The  $\mathbf{p}$ -dependent parameters  $X_{\mathbf{0},\mathbf{p}} = \sum_{\delta} \Delta'_{\delta,\mathbf{0}} e^{-i\mathbf{p}\cdot\delta}$  and  $X_{\mathbf{Q},\mathbf{p}} = \sum_{\delta} \Delta'_{\delta,\mathbf{Q}} e^{-i\mathbf{p}\cdot\delta}$  can both be decomposed into four components by different symmetries.

Now we focus on the SC boundary, where SC orders  $\Delta$ ,  $X_{\mathbf{0},\mathbf{p}}$  and  $X_{\mathbf{Q},\mathbf{p}}$  are small quantities and thus are negligible in the calculations of the normal mean fields. We obtain

$$\rho = \frac{2}{\mathcal{V}} \sum_{\mathbf{p}} (n_{\mathbf{p},-} + n_{\mathbf{p},+}), \quad (3a)$$

$$\rho' = \frac{1}{\mathcal{V}} \sum_{\mathbf{p}} \cos \theta_{\mathbf{p}} \gamma_{\mathbf{p}} (n_{\mathbf{p},-} - n_{\mathbf{p},+}), \quad (3b)$$

$$m = \frac{1}{\mathcal{V}} \sum_{\mathbf{p}} \sin \theta_{\mathbf{p}} (n_{\mathbf{p},-} - n_{\mathbf{p},+}). \quad (3c)$$

Here  $n_{\mathbf{p},\pm}$  is the band-selective momentum distribution function  $[e^{-\xi_{\mathbf{p},\pm}/T_c} + 1]^{-1}$  with “ $\pm$ ” standing for the up-

per and lower bands. The  $s$ -wave symmetric parameter  $\theta_{\mathbf{p}} \in [0, \pi/2)$  is determined by the  $\cot \theta_{\mathbf{p}} = \frac{2\tilde{t}}{Um} \gamma_{\mathbf{p}}$  if  $m \neq 0$  otherwise  $\theta_{\mathbf{p}} \equiv 0$ . And the renormalized dispersion is given by

$$\xi_{\mathbf{p},\pm} = \pm \sqrt{4\tilde{t}^2 \gamma_{\mathbf{p}}^2 + U^2 m^2} - \tilde{\mu}. \quad (4)$$

Solving Eq. 3, we can obtain the normal mean fields  $\rho$ ,  $m$ ,  $\rho'$ , and the renormalized dispersion  $\xi_{\mathbf{p},\pm}$ . Note that these quantities are assumed to be the same on both sides near the SC boundary.

Then we deal with the SC orders, and need to diagonalize the  $4 \times 4$  matrix  $h_{\mathbf{p}}$  in order to construct the SC gap equation. Near  $T_c$ , everything can be approximated up to first order of the SC order parameters. The gap equation turns out to be a *ninth*-order linear system of equations, corresponding to the *nine* independent components for the SC order parameters. By symmetries, the gap equation can be further decomposed into 3rd-order for pure  $s$ -wave pairing, 2nd-order for pure  $d$ -wave pairing, and 2nd-order for two kinds of pure  $p$ -wave pairing. For  $d$ -wave and  $p$ -wave pairings, the gap equation is

$$\begin{bmatrix} X_{\mathbf{0},\varphi} \\ X_{\mathbf{Q},\varphi} \end{bmatrix} = \frac{|V|}{\mathcal{V}} \sum_{\mathbf{p}} \varphi_{\mathbf{p}}^2 \begin{bmatrix} F_{\mathbf{p}}^- + F_{\mathbf{p}}^+ & \sin \theta_{\mathbf{p}} (F_{\mathbf{p}}^+ - F_{\mathbf{p}}^-) \\ \sin \theta_{\mathbf{p}} (F_{\mathbf{p}}^+ - F_{\mathbf{p}}^-) & \sin^2 \theta_{\mathbf{p}} (F_{\mathbf{p}}^- + F_{\mathbf{p}}^+) + 2 \cos^2 \theta_{\mathbf{p}} F'_{\mathbf{p}} \end{bmatrix} \begin{bmatrix} X_{\mathbf{0},\varphi} \\ X_{\mathbf{Q},\varphi} \end{bmatrix}. \quad (5)$$

Here the function  $\varphi_{\mathbf{p}}$  equals to  $\cos p_x - \cos p_y$  for  $d$ -wave

and  $\sin p_x \pm \sin p_y$  for  $p$ -wave pairings. The symmetry-

specified components are defined through  $X_{\mathbf{0},\mathbf{p}} = X_{\mathbf{0},\varphi}\varphi_{\mathbf{p}}$  and  $X_{\mathbf{Q},\mathbf{p}} = X_{\mathbf{Q},\varphi}\varphi_{\mathbf{p}}$ . And  $F$ 's are defined as

$$F_{\mathbf{p}}^{\pm} = \frac{1}{2\xi_{\mathbf{p},\pm}} \tanh \frac{\xi_{\mathbf{p},\pm}}{2T}, \quad (6a)$$

$$F'_{\mathbf{p}} = \frac{1}{\xi_{\mathbf{p},+} + \xi_{\mathbf{p},-}} \frac{1}{2} \left( \tanh \frac{\xi_{\mathbf{p},-}}{2T} + \tanh \frac{\xi_{\mathbf{p},+}}{2T} \right). \quad (6b)$$

According to the condition of existence of nonzero solution to Eq. 5, we can find the critical temperature  $T_c$  for the onset of  $d$ -wave and  $p$ -wave pairing instabilities.

Note that if  $X_{\mathbf{Q},\varphi}$  is not zero, the nonlocal SC orders will be subject to spatial modulation. The sketches of the spatial distribution of the nonlocal SC order  $\Delta'_{\delta,\mathbf{r}}$  for  $d$ -wave and  $p$ -wave pairings is shown in Figure 1. They are similar and closely related to the distribution of  $z$ -spin density  $m_{\mathbf{r}}$ .

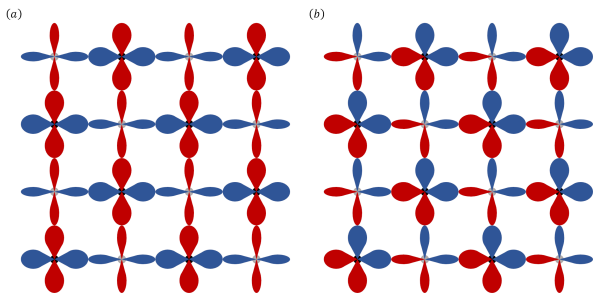


FIG. 1. The sketches of the spatial distribution of the nonlocal SC order  $\Delta'_{\delta,\mathbf{r}}$  (a)  $d$ -wave and (b)  $p$ -wave pairings ( $\varphi_{\mathbf{p}} = \sin p_x + \sin p_y$  here, noting that two kinds of  $p$ -wave are degenerate.) The value of  $\Delta'_{\delta,\mathbf{r}}$  is represented by the “droplet” with its tip at point  $\mathbf{r}$  and tail pointing towards point  $\mathbf{r} + \delta$ , where the absolute value is indicated by the area of the droplet, and the sign by the color, with “-” by dark red and “+” by dark blue.

**Limiting AFM case.** Here we present an analysis in the limiting AFM case where  $Um \gg 4\tilde{t}$ . The large AFM gap confines the physics to a single branch of the band structure, the lower branch if  $\rho < 1$  and the higher branch if  $\rho > 1$ . We only consider the case  $\rho < 1$ . The effective bandwidth  $D$  is then  $\sim 8\tilde{t}^2/Um$ , which is much less than  $8t$  in the noninteracting case. On the other hand, the SC gap equation Eq. 5 is reduced to

$$1 = \frac{|V|}{\mathcal{V}/2} \sum_{\mathbf{p}} \varphi_{\mathbf{p}}^2 F_{\mathbf{p}}^{-}. \quad (7)$$

This equation is not particularly different from the gap equation in conventional superconductors, except that the effective dispersion is extremely narrow, which, however, is indeed the fundamental difference.

To illustrate this point, we introduce a function

$$w_{\mathbf{p}} = \frac{2T_c}{\xi_{\mathbf{p},-}} \tanh \frac{\xi_{\mathbf{p},-}}{2T_c}, \quad (8)$$

and note that  $F_{\mathbf{p},-} = w_{\mathbf{p}}/4T_c$ . Then we can derive the relation  $T_c \sim 0.25|V|\tilde{w}$  from Eq. 7, where the scalar  $\tilde{w}$  can further be proxied by the average  $\bar{w} = \frac{1}{\mathcal{V}/2} \sum_{\mathbf{p}} w_{\mathbf{p}}$ . If the energy scale of the effective bandwidth  $D$  is comparable to  $T_c$ , the value of  $\bar{w}$  will be a constant close to 1, and hence  $T_c \sim 0.25|V|$ . In contrast, for conventional superconductors, the bandwidth is much larger than the Debye frequency which is also much larger than  $T_c$  [22], and thus  $T_c$  is constrained by the McMillan limit [23].

The theoretical analysis in the limiting AFM case reveals the possible high- $T_c$  SC mechanism in the extended Hubbard model: the strong local repulsion  $U$  generates a large AFM gap, which leads to an extremely narrow effective bandwidth  $D$  and thus a linear dependence of  $T_c$  on the nearest-neighbor attraction  $|V|$ . Next, we will numerically verify this mechanism and explore some features on the SC boundary based on Eq. 5.

**Numerical results.** The numerical calculations are all performed on a  $512 \times 512$  lattice in the case  $\rho < 1$  and  $t = 1$  is set as the unit of energy. The parameter range in consideration is based on the experimental results on the cuprate chains [15], where  $U \sim 8t$  and  $|V| \sim t$ . To gain a global understanding of the features of  $T_c$ , we plot its dependence on the doping  $1 - \rho$  for two sets of  $U$  values (4.0, 8.0) and two sets of  $|V|$  values (0.5, 1.0), for  $d$ -wave instability (solid line) and  $p$ -wave (dashed line) instability, as shown in Figure 2. The plot reveals three key features: the curve of  $T_c$  versus doping exhibits a dome shape;  $T_c$  is positively correlated with local repulsion  $U$ , but the relationship is not strong;  $T_c$  demonstrates a positive correlation with the nearest-neighbor attraction  $|V|$ , and the dependence is statistically significant. Besides,  $d$ -wave instability is generally more prevalent than  $p$ -wave instability.

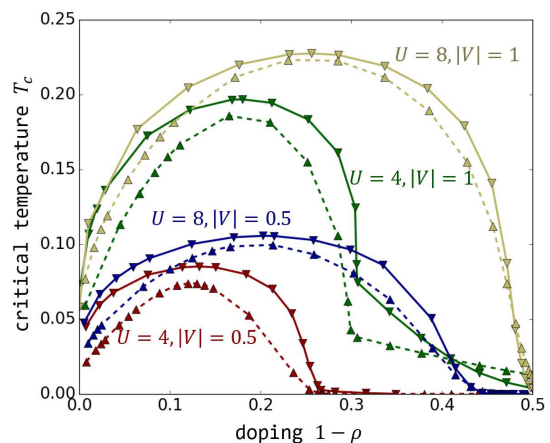


FIG. 2. Critical temperature versus doping for  $d$ -wave instability (solid line) and  $p$ -wave instability (dashed line) at varying values of  $U$  (4.0, 8.0) and  $|V|$  (0.5, 1.0). The plot reveals some features of the dependence of  $T_c$ .

Figure 2 provides a preliminary check of our theoretical analysis. To further verify it, we focus on the dependence of the optimal  $T_c$  on  $U$  and  $|V|$ . The plot of the optimal  $T_c$  for  $d$ -wave instability (solid line) and  $p$ -wave instability (dashed line) versus the inverse local repulsion  $1/U$  at varying values of  $|V|$  (0.5, 1.0, 2.0) is shown in Figure 3a, together with the optimal doping shown in Figure 3b. In order to explore more features, we also plot the effective bandwidth  $D$  (the lower energy band) in Figure 3c, the value of  $\bar{w}$  in Figure 3d, the AFM moment  $m$  in Figure 3e, and the value of  $-X_{\mathbf{Q},\varphi}/X_{\mathbf{0},\varphi}$  in Figure 3f.

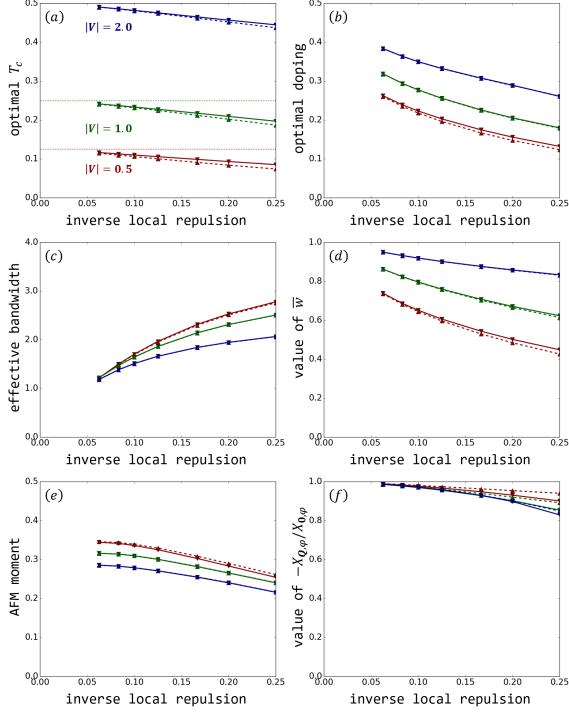


FIG. 3. Plot of the optimal  $T_c$  versus the inverse local repulsion  $1/U$  for  $d$ -wave instability (solid line) and  $p$ -wave instability (dashed line) at varying values of  $|V|$  (0.5, 1.0, 2.0), shown in panel (a). The dotted line refers to the upper bound of  $T_c$ :  $0.25|V|$ . Rest panels are values of quantities at the optimal points: (b) the doping  $1 - \rho$ , (c) the effective bandwidth  $D$ , (d)  $\bar{w}$ , (e) the AFM moment  $m$ , and (f)  $-X_{\mathbf{Q},\varphi}/X_{\mathbf{0},\varphi}$ .

Figure 3a illustrates that  $T_c$  is positively correlated with  $U$  and tends to an upper bound of  $0.25|V|$  as  $U$  is sufficiently large. To understand this property, we need to clarify the following points. First, we can use the relation  $T_c \sim 0.25|V|\bar{w}$  as a reference, since the value of  $\bar{w}$  is limited within  $0.5 - 1.0$ . Second,  $\bar{w}$  is negatively correlated with  $D$  due to that  $\tanh(x) \sim x - \frac{1}{3}x^3$  as  $x$  is small. Third,  $D \sim \frac{8t^2}{Um}$  is nearly proportional to  $1/U$ . Therefore,  $T_c$  is positively correlated with  $\bar{w}$ , negatively correlated with  $D$ , and positively correlated with  $U$ . Besides, Figure 3 also exhibits other properties at the optimal points: as  $U$  increases, the doping increases, the

AFM moment  $m$  increases and tends to a constant, and the value of  $-X_{\mathbf{Q},\varphi}/X_{\mathbf{0},\varphi}$  increases and tends to 1.0.

The plot of the optimal  $T_c$  for  $d$ -wave instability (solid line) and  $p$ -wave instability (dashed line) versus the nearest-neighbor attraction  $|V|$  at varying values of  $U$  (4.0, 8.0, 16.0) is shown in Figure 4, together with the plots of doping, the effective bandwidth  $D$ , the value of  $\bar{w}$ , the AFM moment  $m$ , and the ratio  $-X_{\mathbf{Q},\varphi}/X_{\mathbf{0},\varphi}$ . Remarkably, the optimal  $T_c$  is almost linear in  $|V|$ , which can be understood by the reference relation  $T_c \sim 0.25|V|\bar{w}$  and  $\bar{w} \sim 1$  as  $D$  is comparable to  $T_c$ . Besides, Figure 4 also exhibits other properties at the optimal points: as  $|V|$  increases, the doping increases, the effective bandwidth  $D$  tends to a constant, the AFM moment  $m$  decreases and tends to a constant, and the value of  $-X_{\mathbf{Q},\varphi}/X_{\mathbf{0},\varphi}$  is close to 1.0.

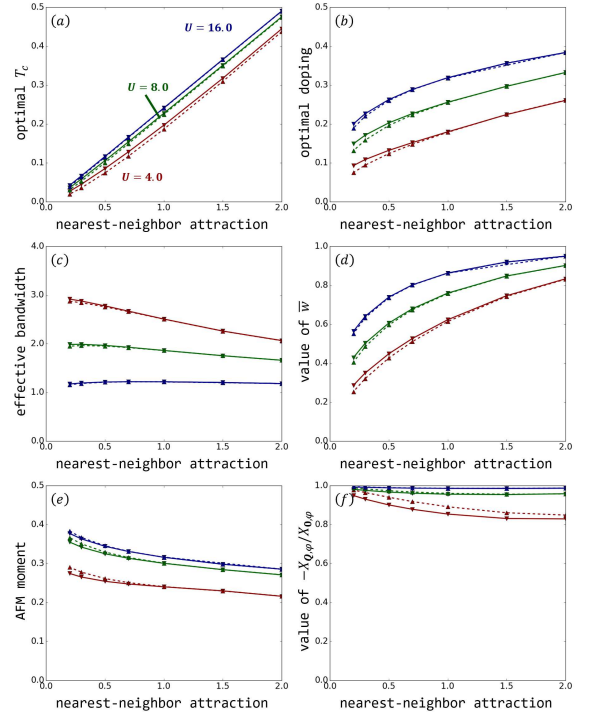


FIG. 4. Plot of the optimal  $T_c$  versus the nearest-neighbor attraction  $|V|$  for  $d$ -wave instability (solid line) and  $p$ -wave instability (dashed line) at varying values of  $U$  (4.0, 8.0, 16.0), shown in panel (a). Rest panels are values of quantities at the optimal points: (b) the doping  $1 - \rho$ , (c) the effective bandwidth  $D$ , (d)  $\bar{w}$ , (e) the AFM moment  $m$ , and (f)  $-X_{\mathbf{Q},\varphi}/X_{\mathbf{0},\varphi}$ .

The numerical results presented in Figures 3 and Figure 4 confirm the roles of local repulsion  $U$  and nearest-neighbor attraction  $|V|$  in the SC problem in the extended Hubbard model. It is evident that  $|V|$  is indispensable for pairing instabilities, and there is a relation  $T_c \sim 0.25|V|$ , provided that the energy scale of the effective bandwidth  $D$  is comparable to  $T_c$ . Meanwhile, the effect of  $U$  is significant as it dramatically narrows down

the value of the  $D$ . Hence, an extremely narrow band and a sufficiently strong attractive potential are two key factors to design high- $T_c$  materials.

**Conclusion and discussion.** To summarize, we investigated the SC problem in the 2D extended Hubbard model under the mean-field framework. Our theoretical analysis and numerical results demonstrate the possible mechanism of high- $T_c$  SC in the extended Hubbard model, which includes two crucial points: (i) the strong local repulsion significantly narrows down the effective bandwidth, and (ii) the critical temperature  $T_c$  shows a linear relationship with the nearest-neighbor attraction if the energy scale of the bandwidth is comparable to  $T_c$ . Our discovery suggests that the design of high- $T_c$  materials should focus on two key factors: a bandwidth that is sufficiently narrow, and a strong attractive potential wherever possible. Moreover, our study reveals that the non-local superconducting order is subject to spatial modulation, which is closely related to the distribution of the spin density. This discovery helps to understand the emergence of the pairing density wave.

Our study qualitatively describes the SC phenomenon on the extended Hubbard model based on the AFM phase assumption within the mean field theory. This assumption can be extended to the general spin density wave phase [24], which is expected to provide a more accurate understanding of the SC properties and to be crucial for understanding stripe phases and pairing density waves. For obtaining better quantitative results and understanding the pseudogap physics, we can turn to more complex and accurate methods such as weak-coupling fluctuation theory [8, 25], dynamical mean field theory [9], and density matrix renormalization group approaches [26].

---

\* zpsun@csrc.ac.cn

† haiqing0@csrc.ac.cn

- [1] J. G. Bednorz and K. A. Müller, *Zeitschrift für Physik B Condensed Matter* **64**, 189 (1986).
- [2] R. Micnas, J. Ranninger, and S. Robaszkiewicz, *Rev. Mod. Phys.* **62**, 113 (1990).
- [3] C. C. Tsuei and J. R. Kirtley, *Rev. Mod. Phys.* **72**, 969 (2000).

- [4] D. J. Scalapino, *Rev. Mod. Phys.* **84**, 1383 (2012).
- [5] J. A. Sobota, Y. He, and Z.-X. Shen, *Rev. Mod. Phys.* **93**, 025006 (2021).
- [6] P. W. Anderson, *Science* **235**, 1196 (1987).
- [7] J. E. Hirsch and S. Tang, *Phys. Rev. Lett.* **62**, 591 (1989).
- [8] Y. M. Vilks and A.-M. S. Tremblay, *Journal de Physique I* **7**, 1309 (1997).
- [9] T. Schäfer, N. Wentzell, F. Šimkovic, Y.-Y. He, C. Hille, M. Klett, C. J. Eckhardt, B. Arzhang, V. Harkov, F.-M. Le Régent, A. Kirsch, Y. Wang, A. J. Kim, E. Kozik, E. A. Stepanov, A. Kauch, S. Andergassen, P. Hansmann, D. Rohe, Y. M. Vilks, J. P. F. LeBlanc, S. Zhang, A.-M. S. Tremblay, M. Ferrero, O. Parcollet, and A. Georges, *Phys. Rev. X* **11**, 011058 (2021).
- [10] E. W. Huang, R. Sheppard, B. Moritz, and T. P. Devereaux, *Science* **366**, 987 (2019).
- [11] H. Kontani, *Reports on Progress in Physics* **71**, 026501 (2008).
- [12] N. E. Bickers, D. J. Scalapino, and S. R. White, *Phys. Rev. Lett.* **62**, 961 (1989).
- [13] M. Qin, C.-M. Chung, H. Shi, E. Vitali, C. Hubig, U. Schollwöck, S. R. White, and S. Zhang (Simons Collaboration on the Many-Electron Problem), *Phys. Rev. X* **10**, 031016 (2020).
- [14] H. Xu, C.-M. Chung, M. Qin, U. Schollwöck, S. R. White, and S. Zhang, Coexistence of superconductivity with partially filled stripes in the hubbard model (2023), arXiv:2303.08376 [cond-mat.supr-con].
- [15] Z. Chen, Y. Wang, S. N. Rebec, T. Jia, M. Hashimoto, D. Lu, B. Moritz, R. G. Moore, T. P. Devereaux, and Z.-X. Shen, *Science* **373**, 1235 (2021).
- [16] Y. Wang, Z. Chen, T. Shi, B. Moritz, Z.-X. Shen, and T. P. Devereaux, *Phys. Rev. Lett.* **127**, 197003 (2021).
- [17] M. Jiang, *Phys. Rev. B* **105**, 024510 (2022).
- [18] D.-W. Qu, B.-B. Chen, H.-C. Jiang, Y. Wang, and W. Li, *Communications Physics* **5**, 257 (2022).
- [19] R. Micnas, J. Ranninger, S. Robaszkiewicz, and S. Tabor, *Phys. Rev. B* **37**, 9410 (1988).
- [20] J. Bardeen, L. N. Cooper, and J. R. Schrieffer, *Phys. Rev.* **108**, 1175 (1957).
- [21] J. R. Schrieffer, *Theory of superconductivity* (CRC press, 2018).
- [22] T. Xiang and C. Wu, *D-wave Superconductivity* (Cambridge University Press, 2022).
- [23] W. L. McMillan, *Phys. Rev.* **167**, 331 (1968).
- [24] M. Kato, K. Machida, H. Nakanishi, and M. Fujita, *Journal of the Physical Society of Japan* **59**, 1047 (1990).
- [25] B. Jankó, J. Maly, and K. Levin, *Phys. Rev. B* **56**, R11407 (1997).
- [26] A. Wietek, Y.-Y. He, S. R. White, A. Georges, and E. M. Stoudenmire, *Phys. Rev. X* **11**, 031007 (2021).